Autoionization emission by electron impact in the $3d$ transition-metal series $_{21}$Sc to $_{29}$Cu

G. Zajac, S. D. Bader, A. J. Arko, and J. Zak*
Materials Science and Technology Division, Argonne National Laboratory, Argonne, Illinois 60439
(Received 28 November 1983)

Autoionization emission associated with direct recombination of the resonant $3p \rightarrow 3d$ transitions have been examined for all the $3d$ transition-metal elements from $_{21}$Sc to $_{29}$Cu. Two characteristic trends with atomic number Z are observed which correlate with those previously reported in the $3p$-electron energy-loss spectra. Firstly, the intensity of this emission decreases with increasing Z. Secondly, the separation of the emission peak from the $3p$ threshold is large (~ 10 eV) toward the beginning of the series ($_{21}$Sc through $_{24}$Cr) and abruptly drops to a few electron volts near the middle of the series ($_{25}$Mn, $_{26}$Fe). This latter reduction in peak separation causes the autoionization and ($M_{2,3}VV$) Auger emission to merge into a single spectral feature. We show for $_{25}$Mn (and $_{22}$Ti) that the two contributions can be separately identified by means of oxygen-dosing experiments. Oxidation dramatically shifts the Auger emission to lower energy leaving the autoionization emission as a separate peak pinned above the $3p$ threshold. These measurements shed light on the spectral details in the $3p$ line shapes of the autoionization and the electron-energy-loss spectra. We report angle-resolved measurements for Cr which show different angular dependences of the emission and absorption processes.

I. INTRODUCTION

Electron spectroscopic investigations of narrow-band systems such as the $3d$ transition metals pose two significant challenges: an understanding of the materials properties *and* an understanding of the interactions of the material with the probe. In the present study and in our recent related publication,[1-3] we focus on the latter, especially as it pertains to effects associated with the $3p \rightarrow 3d$ transition. Interest in the energy-absorption process, represented in atomic-configuration notation as

$$3p^6 3d^N \rightarrow 3p^5 3d^{N+1} , \quad (1)$$

stems from the observation of a curious coexistence of discrete and continuum features in inelastic electron scattering and photoabsorption experiments, as outlined in Refs. 4 and 5. The associated electron-emission process is summarized as

$$3p^5 3d^{N+1} \rightarrow 3p^6 3d^{N-1} + \epsilon f , \quad (2)$$

where ϵf denotes the electron emitted into a continuum state, which occurs predominantly with $l=3$ character. Interest in this latter step is due to the observation that the direct recombination denoted in Eq. (2) can serve as a basis for resonant photoemission enhancements of the $3d$ band.[6] Such effects are observed to be excited by synchrotron radiation as the energy is varied in the vicinity of the $3p$ binding energy.[7,8] We have previously demonstrated the existence of the electron-stimulated analog of this resonant electron-emission process for select $3d$ systems.[1-3] In the present work we present results for all the $3d$ transition metals from $_{21}$Sc through $_{29}$Cu.

Early work on inelastic electron scattering of the $3d$ transition metals by means of transmission electron-energy-loss spectroscopy indicated complex spectral characteristics associated with the $3p \rightarrow 3d$ transition, including variable spectral widths, structures, and intensities.[9] The low-atomic-number elements $_{21}$Sc through $_{24}$Cr exhibit spectra that span tens of electron volts. The main spectral peak is also ~ 10 eV removed from the threshold energy of the $3p$ binding energy, and subsidiary structures such as shoulders appear. The elements $_{25}$Mn through $_{29}$Cu have increasingly less intensity in these spectra, relative to those of the neighboring plasma-type excitations at lower energy loss. The spectra for $_{25}$Mn through $_{29}$Cu are broad, but not as broad as for the lower-Z transition elements, and exhibit a clear asymmetry in line shape with shallower falloff at higher energy-loss values than at low. The main spectral peak is within a few electron volts of threshold, contrary to that for the low-Z elements.

A rudimentary explanation of these spectral trends was presented within an atomic model proposed by Davis and Feldkamp.[4] They considered the atomic multiplet terms associated with the $3p^5 3d^{N+1}$ configurations and the Fano-type interference[10] between these discrete $p \rightarrow d$ excitations and the continuum $d \rightarrow \epsilon f$ excitations. For low-Z elements low-spin coupling was invoked, which gave a very broad distribution of multiplet terms for Cr. For higher-Z values high-spin coupling was invoked, in accord with magnetic observations. The distribution of multiplet terms was sufficiently narrow that they merged into a single peak. The result is the dominance of the Fano asymmetry at high Z, as first recognized by Dietz *et al.*[11] For the rare-earth elements and the corresponding $4d^{10}4f^N \rightarrow 4d^9 4f^{N+1}$ transitions, Dehmer *et al.*[12] have, to a greater extent, convincingly demonstrated the importance of an atomic-multiplet treatment coupled to the discrete-continuum interference effect. This is not surprising, since localized frameworks are much more commonly associated with rare-earth than with transition-metal systems.

From resonant photoemission of the $3d$ metals, the picture that is beginning to emerge is quite analogous to the behavior outlined above. There appears to be a Z dependence to the intensity of the emission at resonance.[6-8] The resonance also is very broad, and "delayed" or removed from the threshold at low Z,[6,8] and narrower, less delayed, and dominated by characteristic Fano-type interference at high Z.[7,13,14] (In addition, for Ni and Cu, two-hole satellites quite clearly play an important role in the photoemission spectra as well.[13-16])

In contrast to these complexities the $3s$ levels give rise to simple and Z-independent behavior.[9] The $3s$-electron energy-loss spectrum has a symmetric peak positioned at the threshold, whose width reflects analyzer-resolution and core-hole lifetime effects. No interesting resonant photoemission enhancement effects have been reported.

The organization of the present paper is as follows. Section II contains experimental details. Results for electron-stimulated autoionization emission, $M_{2,3}VV$ Auger emission, and the $3p$- and $3s$-electron energy-loss spectra for the elements Sc through Cu appear in Sec. III. Detailed comparison of the $3p$-electron energy-loss spectral and autoionization-emission line shapes for Cr appear in Sec. III B. We focus on Cr because the detailed differences between these rather similar spectral line shapes are greatest for Cr.[1] The differences are shown to arise from the strong angular dependences of the absorption and emission processes. In Sec. III C oxidation of Mn results are presented. Mn represents a case where the $M_{2,3}VV$ Auger and autoionization emission spectra merge into one peak. The results demonstrate that chemical means exist to decompose the two physically distinct contributions. This serves as a contrast to the physical decomposition possible for magnetic systems by spin-polarization analyses, as in the Fe-based glass study by Landolt and Mauri[17] that we recently commented on.[2] Ti oxidation results also appear in Sec. III C for comparison to the Mn results. In Sec. IV we conclude with a discussion of interesting experimental and theoretical extensions of the present work. In particular, the need for accurate multiplet-term calculations and experiments related to the resonant photoemission behavior of Ni.

II. EXPERIMENTAL

Polycrystalline samples of $_{21}$Sc to $_{29}$Cu were prepared by mechanical polishing down to 500 Å Al_2O_3 grit. Typically, the sample size was $3\times3\times1$ mm. After installation in a stainless-steel ultrahigh-vacuum system with a base pressure of 4.10^{-11} Torr, equipped with a double-pass cylindrical mirror analyzer (CMA), the samples were routinely sputter-anneal cleaned. The sputtering was achieved with 0.5—3-keV Ar^+-ion bombardment at a pressure of 6.10^{-5} Torr argon having ion beam currents on the order of 5—10 μA/cm.[2] The samples were mounted on Ta strip heaters, which could be resistively heated to temperatures of order 1000 °C. Simultaneous bombardment and annealing (600—800 °C) was used to remove particularly troublesome trace contaminants that segregate to the surface from the bulk. In all cases all major contaminants (C, S, O, and N) were removed to less than 1—2 at. %, as determined by Auger scans taken both immediately prior to and after the spectra presented here.

The double-pass CMA was operated in the variable pass-energy mode with resolution $\Delta E/E\sim0.6\%$. The primary beam energy of the coaxial electron gun was varied from 0.22 to 2 keV for the various spectra reported. Electron-energy-loss spectroscopy (ELS) data were all taken with primary beam energies from 220—225 eV. Broad survey scan widths of 200 eV below the primary beam energy permitted observation of not only the plasmon and M-shell core-level losses, but also the low-energy-emission region where both the MVV Auger transitions and autoionization emission occur (as in Fig. 5). Separate high-quality emission spectra were subsequently taken in energy windows of 20—70 or 25—125 eV at a primary beam energy of 2 keV, with data acquisition times of 10—15 min.

Oxygen-dosing experiments for Ti and Mn were performed by shutting off the electron beam and electron multiplier and exposing the surface to O_2 pressures of 1.10^{-7} to 2.10^{-6} Torr for appropriate times. Data-acquisition time for these latter experiments was only 4 min per dose.

Angle-resolved data for Cr were taken separately in a Vacuum Generators ADES-400 system equipped with a Vista Electronics AA01 spectrometer control unit. This arrangement helped preserve the electron-multiplier life, since the hemispherical analyzer is operated at high transmission in the variable pass-energy mode, with the grid at ground potential. The acceptance cone of the energy analyzer is $\approx4°$. The control unit was computer ramped with a typical spectrum consisting of 15 sweeps of 128 points at 0.25 sec/point. The chamber pressure during measurement was 7×10^{-11} Torr. For the angle-resolved measurements a single crystal of Cr was used, cut with a surface normal $\approx10°$ from [111]. This orientation yielded a maximum surface area given the physical dimensions of the available starting crystal. The cleaning procedure, similar to that used above, consisted of Ar^+-ion bombardment (1 keV at ~10 μA/cm^2 beam current) for 30 min followed by electron-beam heating (from behind the measuring surface) to ≈900 °C for 10 min. A sharp low-energy electron diffraction (LEED) pattern was obtained which confirmed a clean, well-ordered tilted [111] surface. Although no attempt was made to monitor the C or O Auger peaks, it was found that a strong $M_{2,3}VV$ Auger transition only accompanied a relatively clean surface. The measurement geometry is shown in the inset of Fig. 7 with the energy analyzer rotatable in the x-y plane. The electron-beam energy was 300 eV for ELS measurements and 3 keV for the emission measurements.

III. RESULTS

A. Emission and loss spectra

Figure 1 contains schematic representations within the band framework of the autoionization and related Auger processes. Comparison of the two processes provides guidelines as to where to search for autoionization emission relative to where the well-known $M_{2,3}VV$ Auger

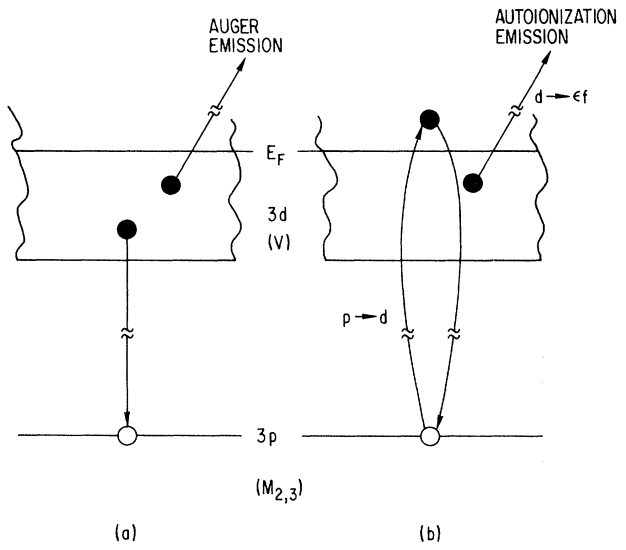

FIG. 1. Comparison of (a) a conventional $M_{2,3}VV$ Auger emission process with (b) the autoionization emission process due to direct recombination of the $p \rightarrow d$ transition, and renormalized by the interference of the $p \rightarrow d$ and $d \rightarrow \epsilon f$ channels.

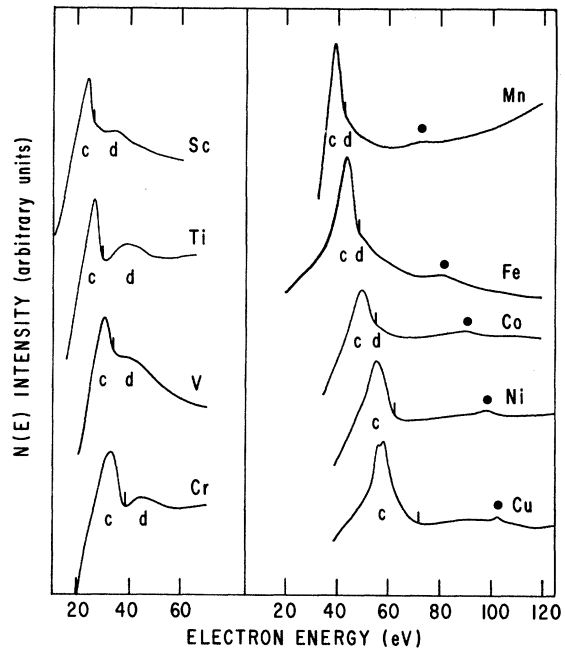

FIG. 2. Low-energy emission region showing the $M_{2,3}VV$ Auger transition, *c*, and the autoionization emission, *d*. The solid circle indicates the weak M_1VV Auger transition.

emission occurs. In Fig. 1(a) the $3p$ core hole was created by the primary electron beam which removes a $3p$ electron from the solid. One $3d$ electron quenches the core hole, and another is simultaneously emitted as the Auger electron, leaving a two-hole final state. In Fig. 1(b) the $3p$ hole was created by the primary electron beam inelastically scattering the $3p$ electron into a $3d$ state. The core hole is quenched by direct recombination of the initial excitation process and simultaneous autoionization emission to an unbound state ϵf in order to conserve energy. Note, that this final state has one hole in the *d* band, as in conventional photoemission. Operationally, the distinguishing feature of the two processes is that the Auger electron always exits with a kinetic energy *less* than the $3p$ binding energy, while the autoionized electron always exits with kinetic energy *greater* than the $3p$ binding energy (aside from a work-function correction). Hence, we search for autoionization emission (abbreviated as ϵf) by looking for features at energies just above the $M_{2,3}VV$ Auger emission.

Figures 2 and 3 show such emission spectra for the $3d$ transition metals taken in undifferentiated and derivative forms, respectively. In Fig. 2 the vertical tick marks denote the $3p$ binding energy minus the 4-eV analyzer work function. The $M_{2,3}VV$ Auger emission is clearly observable below this threshold. The ϵf emission is pronounced in intensity and is well removed above the threshold for Sc through Cr, but barely appears as a high-energy shoulder on the Auger emission for Mn, Fe, and possibly Co, while for Ni and Cu it is not visibly discernible. The ϵf emission for Mn and Fe is somewhat more distinct in the derivative spectra of Fig. 3. [Such derivative spectra have also been published independently for Ti (Ref. 6) and Gd (Ref. 18).] For the elements Mn through Cu the weak M_1VV Auger transitions are also present in the scan range, and are marked by the solid circles. Note also that the spin-orbit splitting of the $3p$ levels is observable in the Cu $M_{2,3}VV$ Auger line shape, but it appears as an asymmetry in the Ni spectrum of Fig. 2.

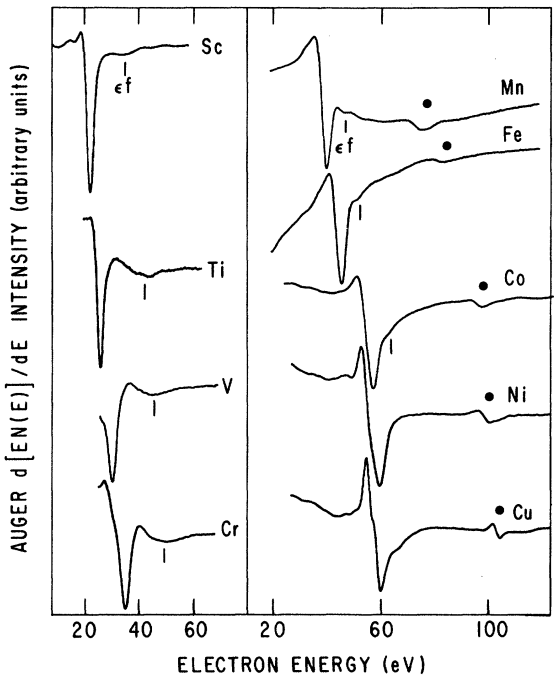

FIG. 3. Derivative spectra for the $3d$ transition-metal series of the emission regions shown in Fig. 2. The low-energy feature is the $M_{2,3}VV$ Auger transition. The vertical tick is the ϵf autoionization emission indicated for $_{21}$Sc to $_{27}$Co. The solid circle indicates the M_1VV Auger transition.

Figure 4 shows the corresponding M-shell core-level loss spectra. As for the emission spectra, the Sc through Cr spectra group into one class with high intensities and strongly delayed onsets, compared to the higher-Z elements. Note that, in Fig. 4, the energy-loss scale increases to the left. The delay of the $3p$ spectral onset causes the absorption features to appear to the left of the $3p$ threshold or to higher energy-loss values. The weak $3s$ core-level losses are denoted by solid circles when they are within the scan range. These losses are symmetric, and positioned at threshold, unlike the interesting $3p$ features. One must conclude that the configuration-interaction coupling that gives rise to the characteristic Fano line shapes is either absent for the $3s$ states, or that the interference between discrete and continuum channels is totally in phase, giving rise to the symmetric line-shape case. The electron-energy-loss spectra in Fig. 4 are in good agreement with the previous results of Ref. 9.

In Fig. 5 the emission and absorption spectra, as in Figs. 2 and 4, respectively, are displayed on a common scale. Figure 5 displays comparisons of the two processes and Z-dependent trends, and was used to normalize the spectra of Figs. 2 and 4. The spectra of Fig. 5 were taken by adjusting the primary electron beam to an energy just above that of the right-hand scale of the plot. By lowering the primary beam energy in this manner, the loss spectrum appears just to the right of the emission spectrum. The spectra are normalized to the plasmon-loss features, labeled a, as in the early transmission ELS work of Ref. 9. The $3p$ core-level losses, labeled b, appear at higher values of energy loss. The vertical ticks represent the $3p$ thresholds based on the x-ray photoemission spectroscopy (XPS) binding energies, and are positioned with respect to the primary (zero-loss) energy. The minor feature below the prominent $M_{2,3}$ loss is the weak M_1 ($3s$) loss. In describing the emission features in Fig. 5, we switch from

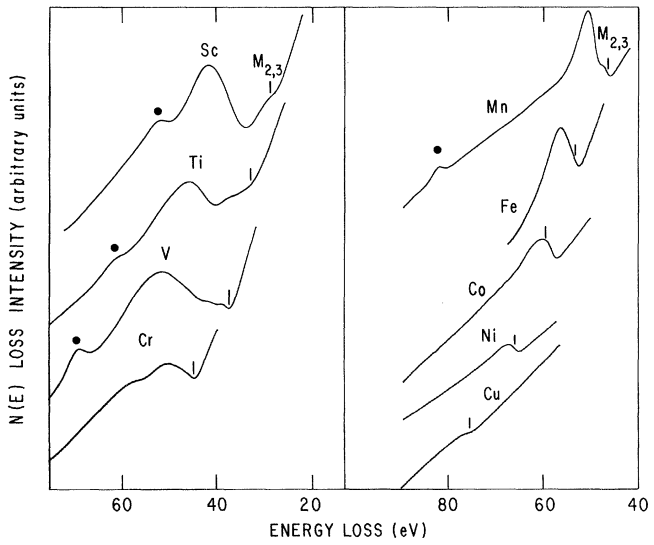

FIG. 4. $M_{2,3}$ core-level energy-loss spectra for $_{21}$Sc to $_{24}$Cu. The $M_{2,3}$ thresholds are marked by the vertical ticks. The solid circles (●) indicate the $M_1(3s)$ energy-loss feature.

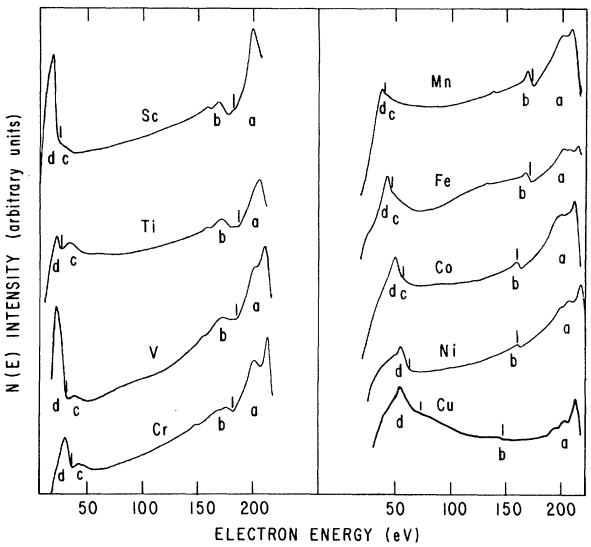

FIG. 5. Electron-energy-loss spectra of the $3d$ transition-metal series ($_{21}$Sc to $_{29}$Cu) taken with a low primary energy of $E_p \cong 225$ eV: a, plasmon region; b, $M_{2,3}$ core-level energy-loss region; c, autoionization emission region; and d, $M_{2,3}VV$ Auger emission region. The vertical ticks indicate the $M_{2,3}$ thresholds.

the energy-loss scale to the kinetic energy scale. The vertical ticks here represent the $3p$ threshold with respect to the kinetic energy scale, adjusted for the analyzer work function, as in Fig. 2. The $M_{2,3}VV$ Auger emission, labeled d, appears below the $3p$ threshold, while the ϵf emission, labeled c, appears above it. The intensity and delayed onset trends with Z can be observed in the loss and emission here, without concern that unspecified normalization procedures can influence the conclusions drawn.

B. Angle-resolved emission and loss spectra for Cr

We have previously presented[1] a detailed comparison of the ϵf emission and $3p$-electron energy-loss spectra line shapes for our V and Cr samples, as well as a comparison of the corresponding data for Fe with existing literature. As we noted then, there is general agreement between thresholds, peak positions, and, most importantly, for V and Cr, there is general agreement between peak intensities. This highlights the corollary nature of the processes as outlined in Eqs. (1) and (2). What we focus on presently is the detailed differences which were especially visible from the Cr comparison. In particular, the loss spectrum exhibited a shoulder $\sim$7 eV further from the threshold than the main peak, while no such corresponding feature was discernible in the otherwise very similar emission spectrum. Since it has been predicted on theoretical grounds from He-gas electron-energy-loss studies, that such a condition can arise from differing angular dependences of the loss and emission spectra, we examined this point to understand the discrepancy. In Fig. 6 we show the angle-resolved $M_{2,3}$ loss spectra for single-crystal chromium using the geometry shown in Fig. 7(c). The angles relative to the sample normal and electron-beam

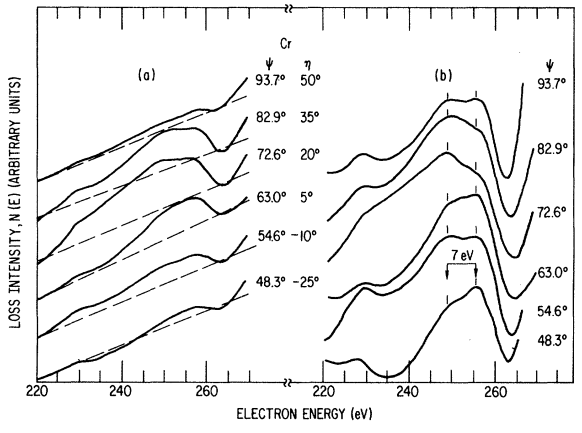

FIG. 6. Angle-resolved spectra of Cr $M_{2,3}$ core-level energy loss, $E_p = 300$ eV. (a) $M_{2,3}$ core-level energy loss (raw data), with arbitrary straight-line background (dashed curve) subtracted and expanded in (b), showing 7-eV splitting believed to be associated with different multiplet terms.

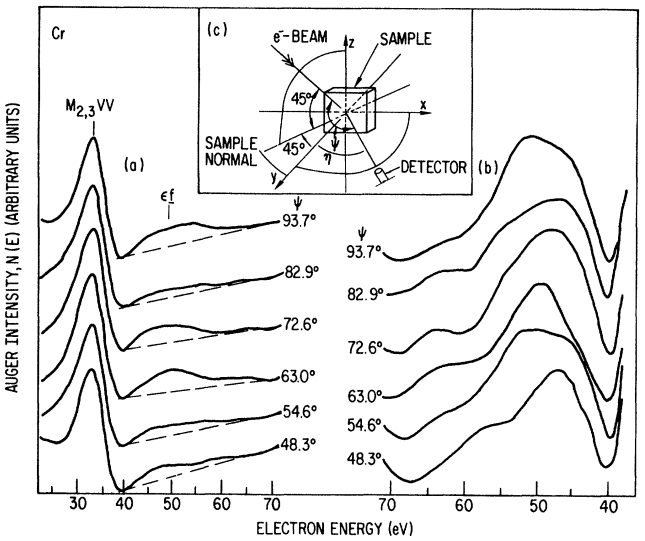

FIG. 7. Angle-resolved emission spectra of Cr showing (a) $M_{2,3}VV$ Auger and autoionization emission regions with arbitrary straight-line background (dashed curve) subtracted, and (b) ϵf the emission region reversed. Note correspondence of multiplet structure with angle-resolved ELS of Fig. 4. The inset (c) shows the scattering geometry with electron beam 45° from sample surface, where ψ is the angle from electron beam to detector, and η is the angle from sample normal to detector.

direction are indicated for each curve. Note that the data were taken on a surface sputtered for 20 min *without* annealing. However, the sample was subsequently annealed and the spectra taken again at angles $\eta = 20°$ and 5° with all features reproducing *exactly*. The dashed lines in Fig. 6(a) are subtracted from the data in Fig. 6(b) to emphasize structure in the spectra and to crudely eliminate background. We note that 7-eV splitting, believed to be associated with different multiplet terms of the $p^5 d^{N+1}$ configuration, as outlined in the Introduction, and we also note the distinct dependence on ψ. (The dependence of the spectral features on ψ was tested by rotating the sample normal by −45°, without observing a change in the spectra at $\psi = 63°$ and $\psi = 72.6°$.)

In Fig. 7 we show the angle-resolved results for the emission region including the $M_{2,3}VV$ Auger transition [Fig. 7(a)]. An arbitrary straight-line background was subtracted from the ϵf emission, and the results are shown in Fig. 7(b) where the energy axis has been reversed in direction and expanded for direct comparison to the $M_{2,3}$ loss spectra of Fig. 6(b). A detailed comparison of the loss and emission spectra again shows striking similarities. Most importantly, the apparent multiplet structure of the ELS data is observable and reflected in the emission region as well, indicating the similar nature of the two processes. It is of interest to note that Barth *et al.*[8] also observed this splitting in their Cr-metal absorption, and yield cross sections taken as a function of photon energy above the $3p$ threshold. This same group has performed related studies of transition-metal vapors[19] as well.

C. Oxygen-induced changes in the emission spectra of Mn and Ti

For the cases of Fe and Mn the ϵf emission is not clearly resolved from the high-energy side of the $M_{2,3}VV$ Auger emission. The two processes, however, can be physically separated for magnetic materials by means of spin-polarization analysis. This was pointed out in our Comment[2] on such an experiment by Landolt and Mauri[17] on an Fe-based glass. A simple explanation is that in polarization analysis the Auger emission can shift away from the ϵf emission by several electron volts since the bottom of the d band is strongly polarized and its emission occurs at lower kinetic energy. The ϵf emission, however, is pinned to being above the $3p$ threshold. Hence, the two emissions separate energetically. We now demonstrate that a chemical method to separate the two contributions exists as well. Oxidation can redistribute the d-band structure such that the Auger emission is shifted down in kinetic energy by as much as 10−15 eV. Again, the ϵf emission is pinned to the $3p$ binding energy, which also shifts upon oxidation, but only by $\lesssim 1-2$ eV, and to higher energies. In addition, since the Z dependence of the ϵf emission intensity is presumably related to the d-band filling, oxidation depopulates the d band, which should act to enhance the ϵf emission.

Oxygen-dosing results for Ti and Mn are shown in Figs. 8(a) and 8(b), respectively. Ti represents an example where the $M_{2,3}VV$ and ϵf emissions are well separated even before oxidation. After oxidation only the ϵf emission is prominent. This is because the metallic $M_{2,3}VV$ Auger signal is removed, and the oxide Auger signal presumably grows at such at low kinetic energy that it is not visible. Bertel *et al.*[6] have seen similar results in derivative-mode experiments, and identified the oxide as TiO_2.

In Fig. 8(b) the more complex oxidation behavior of Mn is shown. Before oxidation the Auger and ϵf emissions are merged into one feature. After oxidation the Auger features distribute throughout the lower-energy region of the spectrum, while the single autoionization emission

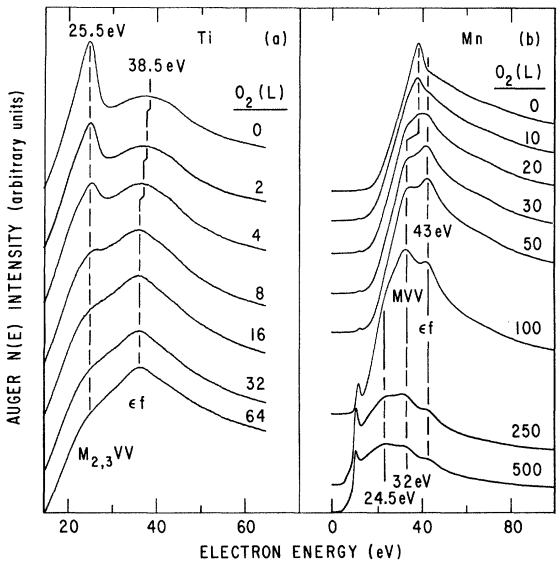

FIG. 8. Oxidation series for (a) $_{22}$Ti and (b) $_{25}$Mn. For Ti the $M_{2,3}VV$ Auger transition is centered at 25.5 eV, and the ϵf emission at 38.5 eV. Note that the Auger signal disappears rapidly upon oxygen dosing, while the ϵf sharpens up and shifts down to 36 eV. For Mn the $M_{2,3}VV$ Auger transition at 38 eV attenuates and shifts to 32 eV upon oxygen dosing, while the ϵf emission grows abruptly and becomes centered at 43 eV. The low-energy shoulder at 24.5 eV which appears at 100 L exposure (1 L$\equiv$1 langmuir$=10^{-6}$ Torr sec) is presumably the interatomic Auger contribution from the oxygen $2p$-like states.

feature remains pinned above the $3p$ binding energy. For Mn it appears that different oxides form as a function of O_2 dosage, while for Ti the maximal-valency oxide is formed directly. These experiments represent yet another example of the reality and importance of the electron-stimulated autoionization emission process in these materials.

IV. DISCUSSION

In this work we have presented the first thorough survey of electron-stimulated autoionization emission in the $3d$ transition metals. An awareness of this process is of general value since the same process occurs in the other transition-metal series[20] and in f-band systems.[12,18,21–24] Also, an appreciation of the inter-relationship of electron- and photon-stimulated emission and absorption experiments makes comparisons to the expanding field of synchrotron-radiation photoemission interesting. Below we discuss two areas—one theoretical, one experimental—where new insights can be obtained by future research.

New theoretical investigations would be of value in understanding the striking similarities in the emission and absorption spectral line shapes. We use the analogy with the core-valence-valence Auger problem. In that case, the line shape often resembles a convolution of the core-level line shape with the valence band folded into itself. For the autoionization emission line shape, to first approximation, a convolution of initial and final states would be represented by the $3p$ loss spectrum and valence band, respectively. Since the d bandwidth[25] is small compared with the loss spectrum, which is presumably dominated by multiplet splittings, the valence band represents an unimportant smearing function, and the loss spectral line shape is preserved in the emission spectrum. This is essentially the conclusion reached by Davis and Feldkamp.[26]

Reliable values of the atomic multiplet terms for the $3d$ metals, in order to further test the applicability of the atomic model, are lacking. Also, correct term assignments are needed to properly interpret spin-polarization data, such as in Ref. 17, as well as resonant photoemission cross-section results.[6–8]

An area of future experimental interest concerns the relationship for Ni between the electron-stimulated autoionization emission and the resonant photoemission cross section of the valence-band region. It is well known that the 6-eV two-hole satellite in Ni goes through a strong Fano-type resonance upon sweeping the photon energy in the vicinity of the $3p$ binding energy.[14,15] The "main line," or conventional one-hole photoemission spectrum of the d band of Ni, shows a weaker antiresonance in the same region.[14,20] The mechanisms for these effects should be due to two-hole Auger emission interference for the satellite and one-hole autoionization emission for the main line. The prediction is that the electron-stimulated emission spectrum should show a weak antiresonance, or negative dip, at energies above those for the $M_{2,3}VV$ Auger emission. In conventional emission spectroscopy such an effect would be difficult to separate from background characterization effect. This would explain our inability to make the identification. However, spin-polarization analysis may be a very powerful tool here, because the background would essentially be automatically eliminated, since it is uniformly polarized.

In the present work we surveyed the autoionization emission process associated with the resonant $3p\rightarrow 3d$ transitions. We examined Z-dependent trends in spectral shape and intensity. We also examined the angular dependences of the emission and absorption processes in Cr, and we found striking, detailed similarities. We demonstrated for the case of Mn, where the autoionization emission merges with the $M_{2,3}VV$ Auger emission, that chemical means exist—by oxygen-dosing experiments to separate the component contributions. We discussed the need for accurate multiplet-term calculations for the $3p^5 3d^{N+1}$ configurations. Finally, we proposed an interesting spin-polarization experiment for Ni that would demonstrate the close relationship between electron- and photon-stimulated emission experiments.

ACKNOWLEDGMENTS

One of the authors (G.Z.) would like to thank L. C. Davis for insightful comments on the autoionization emission intensity. We would also like to thank J. Deh-

mer and U. Fano for useful discussion on the emission process. The technical support of R. J. Friddle and B. Kestel is gratefully acknowledged. Another one of us (S.D.B.) thanks M. Campagna and the Institut für Festkörperforschung der Kernforschungsanlage, Jülich, for their hospitality during the preparation of sections of the manuscript. This work was supported by the U.S. Department of Energy.

---

*Permanent address: Department of Physics, Technion, Israel Institue of Technology, Haifa, Israel.

[1]S. D. Bader, G. Zajac, and J. Zak, Phys. Rev. Lett. 50, 1211 (1983).

[2]G. Zajac, J. Zak, and S. D. Bader, Phys. Rev. Lett. 50, 1713 (1983).

[3]G. Zajac, J. Zak, and S. D. Bader, Phys. Rev. B 27, 6649 (1983).

[4]L. C. Davis and L. A. Feldkamp, Solid State Commun. 19, 413 (1976).

[5]M. B. Stearns and L. A. Feldkamp, *Magnetism and Magnetic Materials—1975 (Philadelphia),* proceedings of the 21st Annual Conference on Magnetism and Magnetic Materials, edited by J. J. Becher, G. H. Lander, and J. J. Rhyne (AIP, New York, 1976), p. 286.

[6]E. Bertel, R. Stockbauer, and T. E., Madey, Phys. Rev. B 27, 1939 (1983).

[7]A. Kakizaki, H. Sugawara, I. Nagahura, Y. Ishikawa, T. Komatsubara, and T. Ishii, J. Phys. Soc. Jpn. 51, 2597 (1981).

[8]J. Barth, F. Gerken, R. L. I. Kibayashi, J. H. Weaver, and B. Sonntag, J. Phys. C 13, 1369 (1980).

[9]J. L. Robins and J. B. Swan, Proc. Phys. Soc. London 76, 857 (1960).

[10]U. Fano, Phys. Rev. 124, 1866 (1961).

[11]R. E. Dietz, E. G. McRae, Y. Yafet, and C. W. Caldwell, Phys. Rev. Lett. 33, 1372 (1974).

[12]J. L. Dehmer, A. F. Starace, U. Fano, J. Sugar, and J. W. Cooper, Phys. Rev. Lett. 26, 1521 (1971).

[13]M. R. Thuler, R. N. Benbow, and Z. Hurych, Phys. Rev. B 26, 669 (1982).

[14]S. J. Oh, J. W. Allen, I. Lindau, and J. C. Mikkelsen, Jr., Phys. Rev. B 26, 4845 (1982).

[15]C. Guillot, Y. Ballu, J. Paigne, J. LeCante, K. P. Jain, P. Thiry, R. Pinchaux, Y. Petroff, and L. M. Falicov, Phys. Rev. Lett. 39, 1632 (1977).

[16]L. C. Davis and L. A. Feldkamp, Phys. Rev. B 23, 6239 (1981).

[17]M. Landolt and D. Mauri, Phys. Rev. Lett. 49, 1783 (1982).

[18]F. Gerken, J. Barth, K. L. I. Kobayashi, and C. Kunz, Solid State Commun. 35, 179 (1980).

[19]E. Schmidt, H. Schröder, B. Sonntag, H. Voss, and H. E. Wetzel, J. Phys. B 16, 2961 (1983); R. Bruhm, E. Schmidt, H. Schröder, and B. Sonntag, *ibid.* 15, 2807 (1982); Phys. Lett. 90A, 41 (1982).

[20]R. E. Dietz, Y. Yafet, G. P. Williams, G. J. Lepeyre, and J. Anderson, Phys. Rev. B 24, 6820 (1981).

[21]R. Haensel, P. Rabe, and B. Sonntag, Solid State Commun. 8, 1845 (1970).

[22]B. Riehl, N. Martensson, D. E. Eastman, A. J. Arko, and O. Vogt, Phys. Rev. B 26, 1842 (1982).

[23]J. A. D. Matthew and S. M. Girvin, Phys. Rev. B 24, 2249 (1981).

[24]E. Bertel, G. Strasser, F. P. Netzer, and J. A. D. Matthew, Surf. Sci. 118, 387 (1982).

[25]V. E. Moruzzi, J. F. Janak, and A. R. Williams, in *Calculated Electronic Properties of Metals* (Pergamon, New York, 1978), pp. 64ff.

[26]L. C. Davis and L. A. Feldkamp, Phys. Rev. B 23, 6239 (1981), and private communication.